



## Full Length Article

Experimental study on the desorption behavior of high-volatile bituminous coals following CO<sub>2</sub> and CH<sub>4</sub> injection at various compositional ratiosJielin Lu, Xuehai Fu <sup>\*</sup>, Junqiang Kang, Ming Cheng, Baoxin Zhang, Haifeng Ji*Key Laboratory of Coalbed Methane Resources and Reservoir Formation Process, Ministry of Education, China University of Mining and Technology, Xuzhou, Jiangsu 221008, China**School of Resources and Geoscience, China University of Mining and Technology, Xuzhou, Jiangsu 221008, China*

## ARTICLE INFO

## ABSTRACT

**Keywords:**  
CO<sub>2</sub>-ECBM  
Different compositional ratios of CO<sub>2</sub>/CH<sub>4</sub>  
Desorption volume  
Desorption strain  
High-volatile bituminous coals

CO<sub>2</sub>-ECBM (Enhanced Coalbed Methane recovery) offers the dual benefits of increasing methane production and reducing carbon emissions through sequestration. Previous studies have primarily focused on the competitive adsorption effects of different gas compositions during the CO<sub>2</sub>-ECBM. However, the dynamic changes in desorption volume, desorption strain, and gas composition for different compositional ratios of CO<sub>2</sub>/CH<sub>4</sub> after injecting CO<sub>2</sub> remain unclear. Therefore, high-volatile bituminous coals from the southern margin of the Junggar Basin are chosen for desorption experiments with five different compositional ratios of CO<sub>2</sub>/CH<sub>4</sub>. Desorption volume, desorption strain, and gas composition of the coal samples are monitored during the desorption process. Finally, the mechanism influencing the dynamic changes in gas composition during desorption is analyzed. The results indicate that as CO<sub>2</sub> concentration increases, both desorption volume and desorption strain correspondingly increase. At the same desorption volume, a higher CO<sub>2</sub> concentration results in greater desorption strain. For different compositional ratios of CO<sub>2</sub>/CH<sub>4</sub>, CH<sub>4</sub> concentration gradually decreases while CO<sub>2</sub> concentration gradually increases over desorption time. The concentration of the desorption gas is influenced by the initial CO<sub>2</sub> concentration and the pore structure. Specifically, higher initial CO<sub>2</sub> concentrations, better pore opening, and more developed mesopores and macropores lead to greater changes in composition concentrations during desorption. Different concentrations of CO<sub>2</sub> all promote CH<sub>4</sub> production, with higher CO<sub>2</sub> concentrations enhancing CH<sub>4</sub> production efficiency more significantly, especially for samples that are more difficult to produce. The research findings can provide guidance for the efficient production of CBM after CO<sub>2</sub> injection.

## 1. Introduction

CO<sub>2</sub>-ECBM (Enhanced Coalbed Methane recovery) is one of the key methods for enhancing the production efficiency of coalbed methane (CBM) wells while simultaneously sequestering CO<sub>2</sub> [1,2]. During the early stages of CO<sub>2</sub>-ECBM, CH<sub>4</sub> is primarily driven, but as the injection time increases, the process becomes dominated by displacement. Therefore, implementing well shut-in measures during CO<sub>2</sub> injection can be beneficial for improving CH<sub>4</sub> recovery [3]. Extensive research has mainly focused on fundamental theories. On the one hand, coal seams have a higher affinity for adsorbing CO<sub>2</sub> compared to CH<sub>4</sub>, making CO<sub>2</sub> injection favorable for increasing the proportion of CH<sub>4</sub> in the produced gas [4–6]. On the other hand, coal seams preferentially desorb adsorbed CH<sub>4</sub>. Under the same desorption pressure conditions, the amount of non-desorbable CO<sub>2</sub> is significantly higher than that of CH<sub>4</sub>, thereby

achieving effective CO<sub>2</sub> sequestration [7–9].

In multicomponent CBM wells, the differential desorption of various gas compositions under reservoir conditions significantly impact CH<sub>4</sub> production. In coalfields such as the Sydney Coalfield, the Upper Silesian Coalfield, and the Ruhr Coalfield, where the coal reservoirs contain high concentrations of CO<sub>2</sub>, the production rate and recovery of CH<sub>4</sub> are higher during extraction [10]. The Illawarra Coalfield and the Bowen Basin in Australia have experienced multiple large-scale releases of CH<sub>4</sub> due to the influence of CO<sub>2</sub> in the coal seams [5]. In areas such as Miquan on the southern margin of the Junggar Basin in Xinjiang, the CO<sub>2</sub> concentration in coal reservoirs is as high as 40 %, and the development of CBM wells has been effective. As production time increases, there is a trend of gradually increasing CO<sub>2</sub> concentration in the output of multicomponent CBM wells [11,12].

With the development of ECBM technology, injecting CO<sub>2</sub> into coal

\* Corresponding author at: School of Resource and Geosciences, China University of Mining and Technology, Xuzhou, Jiangsu 221116, China.  
E-mail address: [fuxuehai@cumt.edu.cn](mailto:fuxuehai@cumt.edu.cn) (X. Fu).

seams to increase the CO<sub>2</sub> composition proportion is considered an effective method to improve CH<sub>4</sub> recovery and carbon sequestration [5,10,13]. In the Ishikari Coalfield of Hokkaido, Japan, a single-well CO<sub>2</sub> injection test was conducted. The CBM well resumed production after CO<sub>2</sub> injection and a 21-day shut-in period. The gas production increased threefold, but CH<sub>4</sub> still accounted for more than 80 % of the produced gas. In multi-well CO<sub>2</sub> injection tests, the production enhancement effect became more pronounced with the increased amount of CO<sub>2</sub> injected [13,14]. In 2020, a CO<sub>2</sub>-ECBM trial was conducted in the Qinshui Basin, China, where 1690.36 tons of CO<sub>2</sub> were injected, accounting for 8.61 % of the total resources of the injection well. The maximum production enhancement reached 46.85 %, with CH<sub>4</sub> comprising over 98 % of the produced gas [2,15]. In physical simulations of the desorption process with various CH<sub>4</sub>/CO<sub>2</sub> composition ratios, various bituminous coal samples showed an initially slow and then rapid desorption rate for CO<sub>2</sub>, with the CO<sub>2</sub> concentration in the desorbed gas always lower than the original ratio, whereas CH<sub>4</sub> exhibited the opposite characteristics in both desorption rate and concentration [16]. Similarly, in studies on the desorption characteristics with various CH<sub>4</sub>/CO<sub>2</sub> composition ratios and evaluations of CO<sub>2</sub> sequestration potential, CH<sub>4</sub> consistently exhibited preferential desorption. Moreover, a higher CO<sub>2</sub> concentration favored increased CH<sub>4</sub> recovery and enhanced CO<sub>2</sub> sequestration potential [17].

The goal of CBM development is CH<sub>4</sub>, but different non-hydrocarbon gases have varying degrees of inhibitory or promotive effects on CBM production [9,18,19]. There is extensive research on CO<sub>2</sub> injection fracturing for enhancing CBM production [20], with limited studies on the production characteristics of different compositions during secondary production after CO<sub>2</sub> injection displacement. The secondary production process after CO<sub>2</sub> injection displacement is characterized by the competitive desorption and co-migration of different composition gases. The differences between the compositions cause mutual influence during desorption and migration. There are few reports on the changes in the composition of the produced gas over time, especially in terms of quantitative concentration analysis. Focusing on high-volatile bituminous coals from Xinjiang, we conducted physical simulation experiments on the desorption with different CH<sub>4</sub>/CO<sub>2</sub> composition ratios. The aim is to detect the desorption strain of coal samples and the concentration changes of gas compositions during the desorption process, to gain a deeper understanding of the mechanisms influencing the dynamic concentration changes of CBM compositions during secondary production after CO<sub>2</sub> injection. This study seeks to provide theoretical guidance for the efficient development of secondary production after CO<sub>2</sub> injection.

## 2. Sample properties and testing methods

### 2.1. Basic properties of samples

The experimental samples were collected from Wudong Coal Mine (WD), Dahuangshan Coal Mine (DHS), Liuhuanggou Coal Mine (LHG), and Xiaogangou Coal Mine (XGG) on the southern margin of the Junggar Basin. Large blocks (30 × 30 × 30 cm) of fresh coal samples were immediately sealed upon collection from the coal mining faces to prevent oxidation and moisture loss. Upon arrival at the laboratory, standard cylindrical coal specimens of φ25 × 50 mm were drilled, and peripheral crushed samples were taken for basic properties tests. The reflectance of vitrinite ( $R_{o,\max}$ ) and macerals are determined according to ISO17246-2005. Proximate analysis is performed according to ISO 7404-5-2009. The coal composition, moisture content ( $M_{ad}$ ), ash yield ( $A_d$ ), and volatile matter yield ( $V_{daf}$ ) of the four coal samples showed differences (Table 1). WD and DHS coal samples are predominantly vitrinite-rich, followed by inertinite-rich compositions, while LHG and XGG coal samples are primarily inertinite-rich, with vitrinite-rich compositions following.

The pore structure of coal is crucial for the occurrence and migration of CBM [21,22]. In this study, the pore structure of different samples is

**Table 1**  
Test results of basic properties of coal samples.

Coal samples	$R_{o,\max}/\%$	Proximate analysis /%			Macerals /%		
		$M_{ad}$	$A_d$	$V_{daf}$	$V$	$I$	$E$
WD	0.61	3.82	2.83	34.96	58.00	41.40	0.60
DHS	0.62	1.46	4.12	38.08	60.80	37.49	1.71
LHG	0.62	1.56	4.55	23.84	6.80	92.52	0.68
XGG	0.67	0.80	10.89	34.41	35.22	63.53	1.25

$M_{ad}$ -air drying base moisture content;  $A_d$ -dry ash yield;  $V_{daf}$ -dry ash-free volatile yield;  $V$ -Vitrin;  $I$ -Inertinite;  $E$ -Exinite.

characterized using the advantages of high-pressure mercury intrusion and low-temperature nitrogen adsorption. Pores are classified according to the Hodot decimal system, namely micropores (<10 nm), transitional pores (10–100 nm), mesopores (100–1000 nm), and macropores (>1000 nm). The results show significant differences in pore structure among different samples. Specifically, WD, LHG, and XGG samples exhibit relatively well-developed meso- and macropores, with meso- and macropores accounting for over 96 % of the total pore volume in LHG samples. In contrast, DHS samples have a smaller proportion of meso- and macropores, accounting for only 44 % of the total pore volume (Table 2, Fig. 1).

### 2.2. Desorption experiment

#### 2.2.1. Experimental equipment

The experimental setup for desorption consists of a self-designed desorption strain system, capable of applying confining pressure and temperature control to standard coal column samples (φ25 × 50 mm) (Fig. 2). The system comprises six main modules: the gas supply module, core holder module, stress loading-unloading module, gas collection module, data acquisition module, and gas composition detection module.

- (1) The gas supply system primarily consists of gas cylinders and pressure regulators. In this experiment, pure gases (100 % CH<sub>4</sub> and 100 % CO<sub>2</sub>) as well as different compositional ratios of CO<sub>2</sub>/CH<sub>4</sub> (25 % CO<sub>2</sub> + 75 % CH<sub>4</sub>, 50 % CO<sub>2</sub> + 50 % CH<sub>4</sub>, 75 % CO<sub>2</sub> + 25 % CH<sub>4</sub>) are used.
- (2) The core holder device is designed for standard coal column samples of φ25 × 50 mm. A temperature control device is integrated into the core holder device, enabling precise temperature adjustment within the range of 293.15–373.15 K with an accuracy of 0.1 K. Temperature monitoring is conducted throughout the entire experiment to ensure temperature consistency.
- (3) The stress loading-unloading module primarily consists of a set of constant-pressure pump, capable of providing stable confining pressure within the range of 0–40 MPa for the standard coal column samples in the experiment.
- (4) The gas collection system is based on the principle of water displacement. Since CO<sub>2</sub> gas is soluble in water, the collected gas is placed in a NaHCO<sub>3</sub> saturated solution to prevent dissolution.
- (5) The data acquisition system mainly consists of a computer, a static strain gauge, pressure sensors, and a liquid level gauge.

**Table 2**  
Pore volume and proportion of different pore sizes.

Coal samples	Micropores and transition pores		Mesopores and macropores	
	pore volume/ $\text{cm}^3 \cdot \text{g}^{-1}$	pore volume ratio/%	pore volume/ $\text{cm}^3 \cdot \text{g}^{-1}$	pore volume ratio/%
WD	0.0039	28.0 %	0.0099	72.0 %
DHS	0.0066	55.9 %	0.0052	44.1 %
LHG	0.0033	3.6 %	0.0867	96.4 %
XGG	0.0038	20.5 %	0.0147	79.5 %

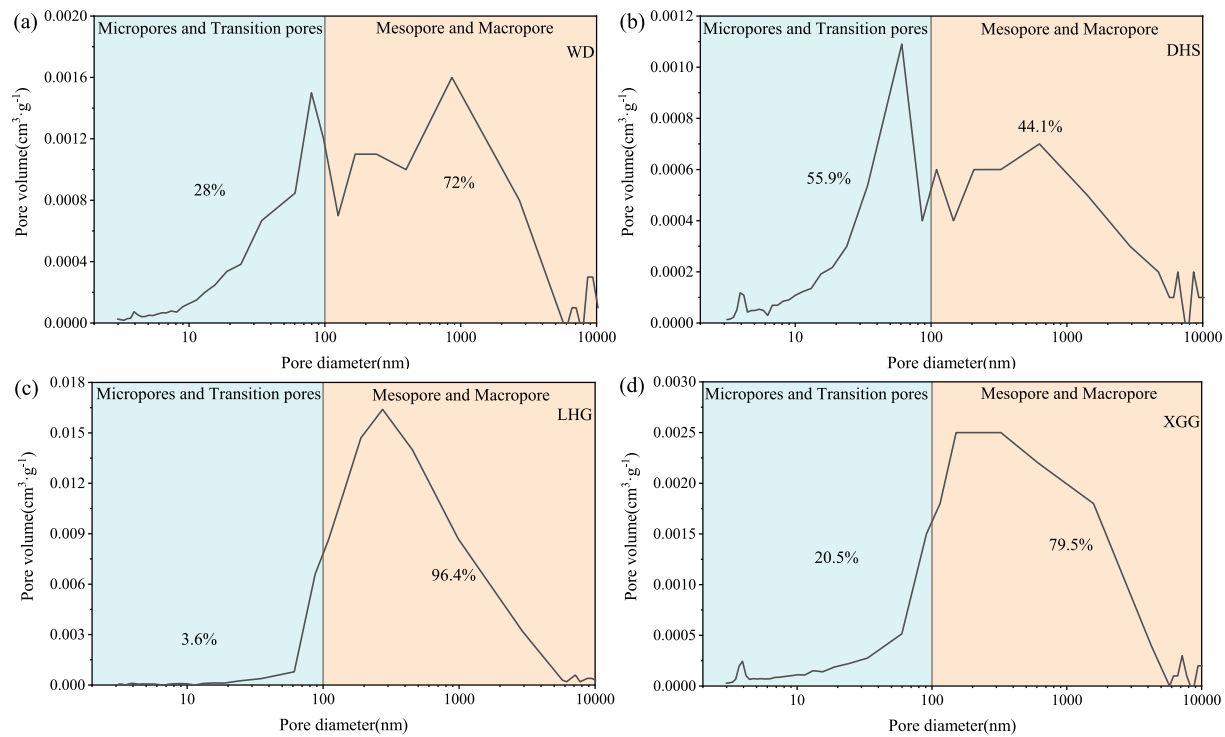


Fig. 1. The fractional pore volumes at different pore size ranges.

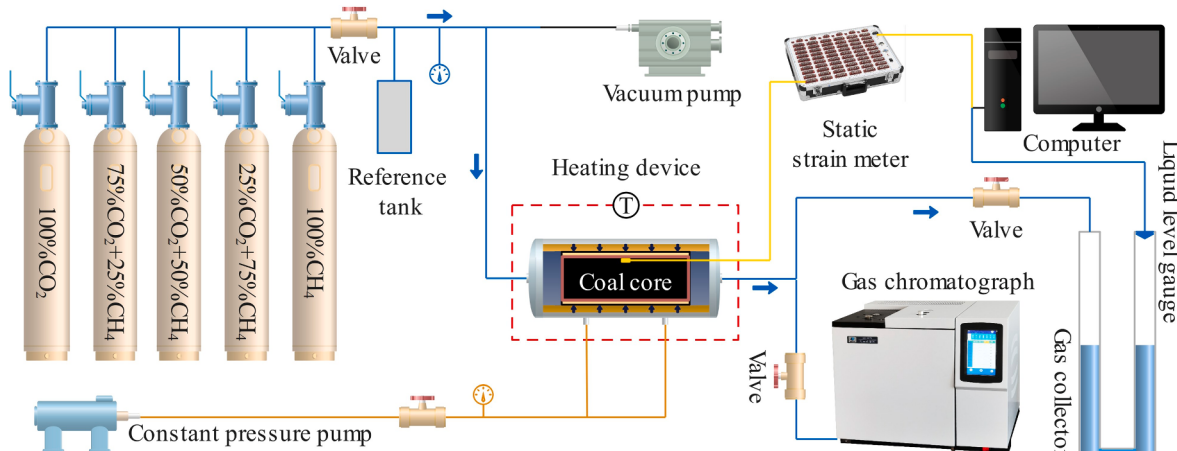


Fig. 2. Schematic diagram of flow simulation test for CBM production process.

During the experiment, the strain gauge is attached to the smooth surface of the coal sample without developed cracks. The strain gauge automatically collects the deformation of the sample during the experiment. The liquid level gauge is used for precise detection of the volume of desorbed gas during the desorption process.

- (6) The gas composition detection system mainly consists of the Thermo TRACE 1300 series gas chromatograph, capable of real-time gas composition detection of the desorbed gases.

### 2.2.2. Experimental procedure

To investigate the production characteristics during the desorption process of different gas compositions, desorption strain experiments are conducted to study the desorption behavior of coal samples under identical confining pressure. In this experiment, different samples are subjected to the same confining pressure and gas pressure. The confining

pressure is set at 8 MPa, while the temperature is maintained at 303.15 K. During the experiment, strain gauges are attached to the smooth coal matrix surface without developed cracks to ensure tight bonding. The deformation characteristics of the coal are monitored in real-time using a static strain gauge, with data collected every 0.5 s. A liquid level gauge is used to continuously monitor the liquid level in the measuring cylinder, with data collected every 2 s, to ensure accurate measurement of desorbed gas volume.

- (1) The coal column sample, with strain gauges already attached, is carefully placed into the core holder. A confining pressure of 8 MPa is steadily applied, while the temperature is maintained at a constant 303.15 K throughout the entire experiment.
- (2) After applying confining pressure to the coal sample, the entire experimental system becomes a sealed unit. Vacuum is applied to the entire system to eliminate the influence of other gases, and

different compositions ratios of  $\text{CO}_2/\text{CH}_4$  at a constant pressure of 6 MPa are introduced. This allows the sample to adsorb continuously for 24 h, reaching a presumed adsorption equilibrium state.

- (3) The desorption experiment begins by closing the inlet valve and opening the outlet valve, with the desorption outlet pressure set at 1 atmosphere (0.1 MPa). The desorption process is lasted for 6 h, during which the desorbed gas volume and coal matrix strain are monitored in real-time. Twelve gas sampling points are set at the following intervals: 0 min, 10 min, 20 min, 40 min, 60 min, 90 min, 120 min, 150 min, 200 min, 260 min, 320 min, and 360 min. Gas composition is analyzed for each of these time points.
- (4) The samples from the previous step underwent low-temperature heating to ensure the complete desorption of adsorbed gases from the coal samples. Different compositions ratios of  $\text{CO}_2/\text{CH}_4$  are then introduced, and the experiments are repeated following the previously outlined steps. After each sample experiment, the experimental apparatus is recalibrated to ensure accuracy.

### 3. Results

This study primarily compares the desorption volume and desorption strain of different samples under different compositions ratios of  $\text{CO}_2/\text{CH}_4$ , as well as the variations of gas compositions over desorption time.

#### 3.1. Desorption volume

There is a significant difference in the desorption volume during the desorption process of different samples with different compositions ratios of  $\text{CO}_2/\text{CH}_4$ . For the WD sample, the maximum desorption volume for different compositions ratios of  $\text{CO}_2/\text{CH}_4$  (100 %  $\text{CO}_2$ , 75 %  $\text{CO}_2 + 25\% \text{CH}_4$ , 50 %  $\text{CO}_2 + 50\% \text{CH}_4$ , 25 %  $\text{CO}_2 + 75\% \text{CH}_4$ , 100 %  $\text{CH}_4$ ) are  $17.56 \text{ cm}^3 \cdot \text{g}^{-1}$ ,  $15.10 \text{ cm}^3 \cdot \text{g}^{-1}$ ,  $12.37 \text{ cm}^3 \cdot \text{g}^{-1}$ ,  $11.30 \text{ cm}^3 \cdot \text{g}^{-1}$ , and  $8.63 \text{ cm}^3 \cdot \text{g}^{-1}$ , respectively. The desorption volume for LHG and XGG samples

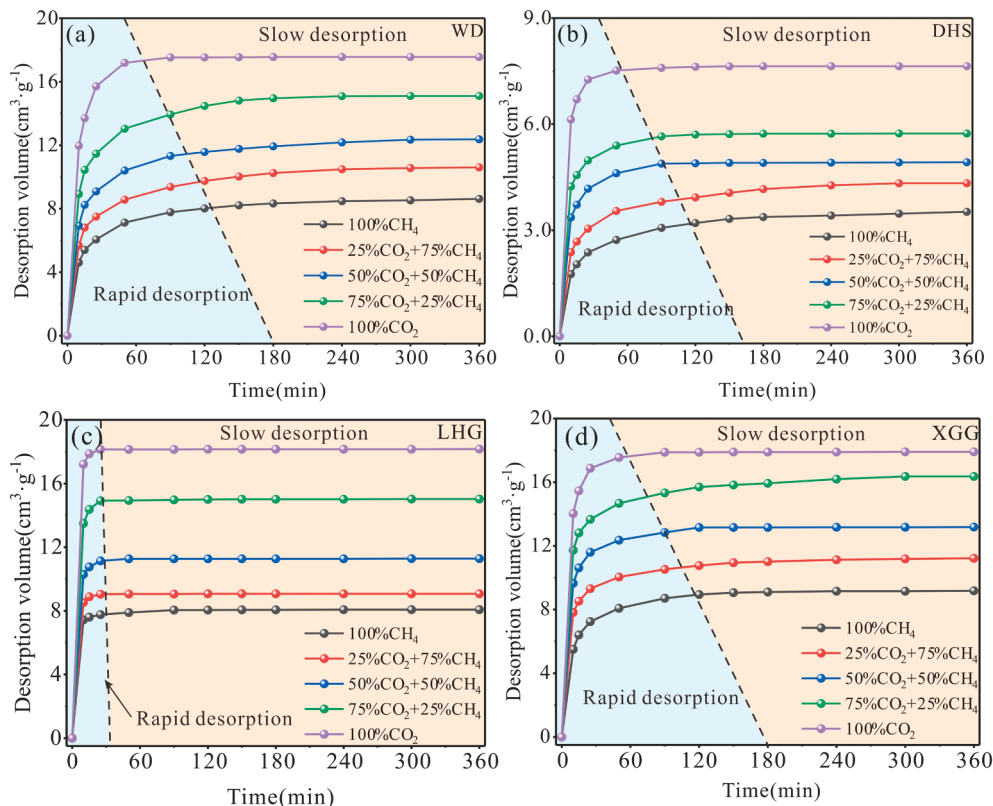


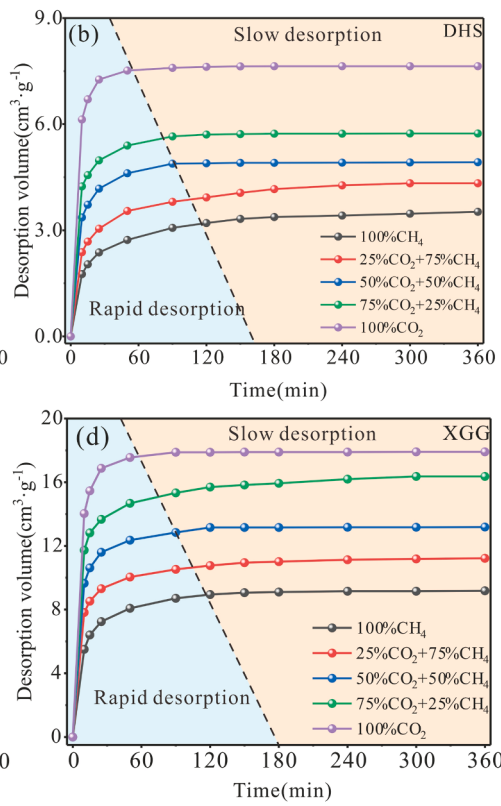
**Fig. 3.** Desorption curves for different compositions ratios of  $\text{CO}_2/\text{CH}_4$ .

under different compositions ratios of  $\text{CO}_2/\text{CH}_4$  are similar to those of the WD sample (Fig. 3a, c, d). However, the desorption volume of DHS sample is significantly smaller than the above three samples, with the desorption volume of 100 %  $\text{CO}_2$  being only  $7.64 \text{ cm}^3 \cdot \text{g}^{-1}$  and that of 100 %  $\text{CH}_4$  being  $3.52 \text{ cm}^3 \cdot \text{g}^{-1}$  (Fig. 3b). For the same sample, the desorption volume consistently followed the trend: 100 %  $\text{CO}_2 > 75\% \text{CO}_2 + 25\% \text{CH}_4 > 50\% \text{CO}_2 + 50\% \text{CH}_4 > 25\% \text{CO}_2 + 75\% \text{CH}_4 > 100\% \text{CH}_4$ . There is no obvious linear relationship between the desorption volumes and  $\text{CO}_2$  concentrations. The desorption volumes under the 100 %  $\text{CO}_2$  and 75 %  $\text{CO}_2 + 25\% \text{CH}_4$  conditions are significantly higher (Fig. 3).

The desorption processes of different samples under different compositions ratios of  $\text{CO}_2/\text{CH}_4$  exhibited difference, characterized by an initial rapid desorption phase followed by a slower desorption phase. The desorption rates of WD, DHS, and XGG samples under different compositions ratios of  $\text{CO}_2/\text{CH}_4$  are significantly lower than those of the LHG sample. For the LHG sample, the rapid desorption phase is completed within 30 min across different compositions ratios of  $\text{CO}_2/\text{CH}_4$ , with a rapid increase in desorption volume (Fig. 3c). In contrast, the WD, DHS, and XGG samples do not complete the rapid desorption phase until around 180 min under different compositions ratios of  $\text{CO}_2/\text{CH}_4$  (Fig. 3a, b, d). For the same sample, higher  $\text{CO}_2$  concentrations led to rapider desorption, which is related to the smaller kinetic diameter of  $\text{CO}_2$  molecules [5,23]. This will be further explained in the context of effective diffusivity in the following sections.

#### 3.2. Desorption strain

During the desorption process, different samples exhibit a trend of desorption strain decreasing rapidly at first and then slowly (Fig. 4). Specifically, for the WD, DHS, and XGG samples, the desorption strain shows a rapid decrease phase around the first 120 min, followed by a slow decrease phase after 120 min (Fig. 4a, b, d). In contrast, for the LHG sample, the desorption strain rapidly decreases until around 60 min,



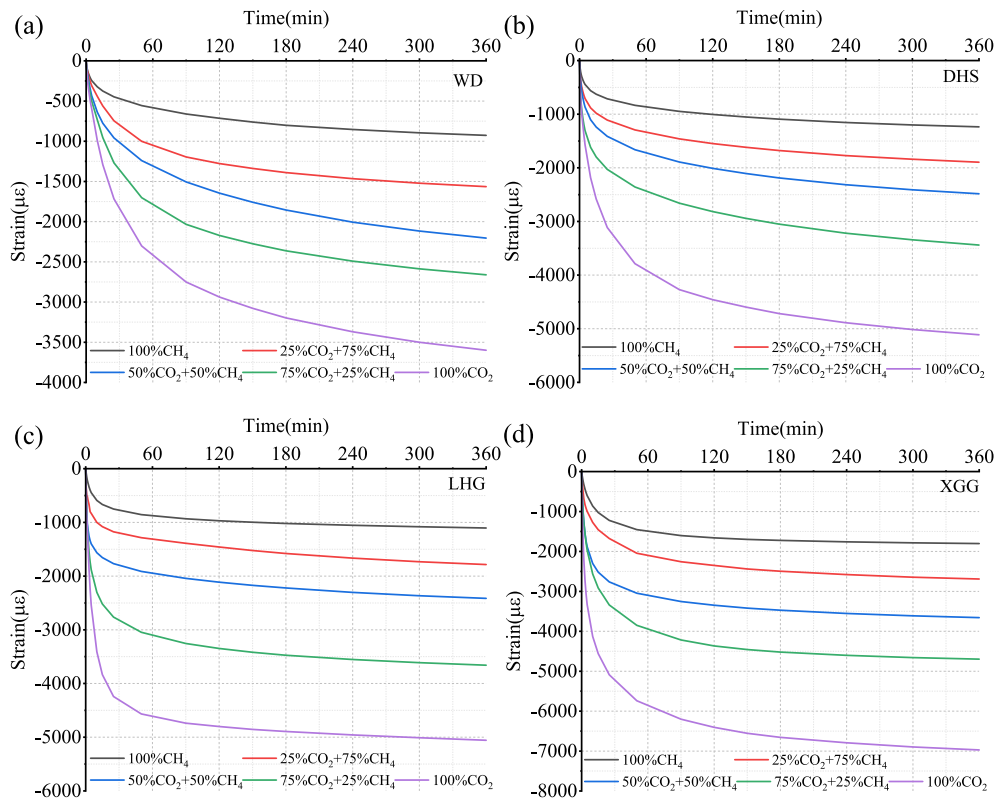


**Fig. 4.** Desorption strain curves for different compositions ratios of  $\text{CO}_2/\text{CH}_4$ .

followed by a gradual decrease (Fig. 4c). The inflection points of desorption strain for different samples do not entirely correspond to those of desorption volume, indicating hysteresis in desorption behavior. For the same sample, the desorption strain under different compositions ratios of  $\text{CO}_2/\text{CH}_4$  shows that the higher the  $\text{CO}_2$  concentration, the greater the desorption strain (Fig. 4).

Many studies have shown a positive correlation between the adsorption/desorption volume and the induced strain [24–26]. In this experiment, different coal samples show significant differences in desorption volume and desorption strain. For example, the DHS sample has much lower desorption volumes for different compositions ratios of  $\text{CO}_2/\text{CH}_4$  compared to the other three samples, with  $\text{CO}_2$  desorption volume of less than  $8 \text{ cm}^3 \cdot \text{g}^{-1}$ , yet its desorption strain reach  $5112.67 \mu\epsilon$ , which is significantly higher than that of the WD and LHG samples. This indicates a substantial difference in deformation capacity among the samples. Notably, all samples exhibit a significant hysteresis effect in desorption strain. The desorption volumes reach maximum values under at 360 min, while the desorption strain continue to increase (Fig. 4). The influencing factors are complex and will be discussed in future research.

### 3.3. Changes in gas compositions

The trends in gas composition changes for different samples under different compositions ratios of  $\text{CO}_2/\text{CH}_4$  are generally consistent. With increasing desorption time, the  $\text{CO}_2$  concentration tends to increase initially and then gradually stabilize, while the  $\text{CH}_4$  concentration shows the opposite trend (Fig. 5). For example, under the condition of 25 %  $\text{CO}_2 + 75 \% \text{CH}_4$ , the WD sample exhibits a decrease in  $\text{CH}_4$  concentration from 84.37 % at the beginning of desorption to 75.66 % at the end of desorption, while the corresponding  $\text{CO}_2$  concentration increases from 15.63 % to 24.34 %. Similarly, under the conditions of 50 %  $\text{CO}_2 + 50 \% \text{CH}_4$  and 75 %  $\text{CO}_2 + 25 \% \text{CH}_4$ , there is a decrease in  $\text{CH}_4$  concentration and an increase in  $\text{CO}_2$  concentration (Fig. 5a, b, c). The desorption trends of gas composition concentrations for the DHS and

XGG samples are consistent with those of the WD sample. Specifically, under different compositions ratios of  $\text{CO}_2/\text{CH}_4$ , the  $\text{CO}_2$  concentration gradually increases with desorption time, while the  $\text{CH}_4$  concentration gradually decreases (Fig. 5d, e, f, j, k, l). However, the desorption patterns of gas composition concentrations for the LHG sample differ significantly from those of the other three samples. Under the three different compositions ratios of  $\text{CO}_2/\text{CH}_4$ , the LHG sample shows an initial increase in  $\text{CO}_2$  concentration during the 0–20-minute period, followed by a gradual decrease after 20 min of desorption. The trend in  $\text{CH}_4$  concentration change is opposite to that of  $\text{CO}_2$  concentration (Fig. 5g, h, i).

The trends in gas composition changes under different compositions ratios of  $\text{CO}_2/\text{CH}_4$  are similar for the WD, DHS, and XGG samples. However, there are still differences in gas composition changes among different samples or under different compositions ratios of  $\text{CO}_2/\text{CH}_4$  for the same sample. For example, the concentration of the WD sample changes rapidly in the early stages and stabilizes later, while the concentrations of the DHS and XGG samples change more gradually throughout the desorption process. On the other hand, the LHG sample exhibits rapid concentration changes in the early stages, followed by a trend opposite to that of the other three samples in the later stages. These differences will be further discussed in the subsequent sections. Throughout the entire desorption process, the  $\text{CH}_4$  concentration remained higher than the initial concentration in the early stages of desorption, which also reflects the performance of  $\text{CO}_2$  injection in improving  $\text{CH}_4$  recovery.

## 4. Discussion

This study primarily discusses the characteristics of changes in composition concentrations during the desorption process of different compositions ratios of  $\text{CO}_2/\text{CH}_4$ , as well as the influencing factors of diffusion. Furthermore, it analyzes the production characteristics of  $\text{CH}_4$  under different compositions ratios of  $\text{CO}_2/\text{CH}_4$  and explores its

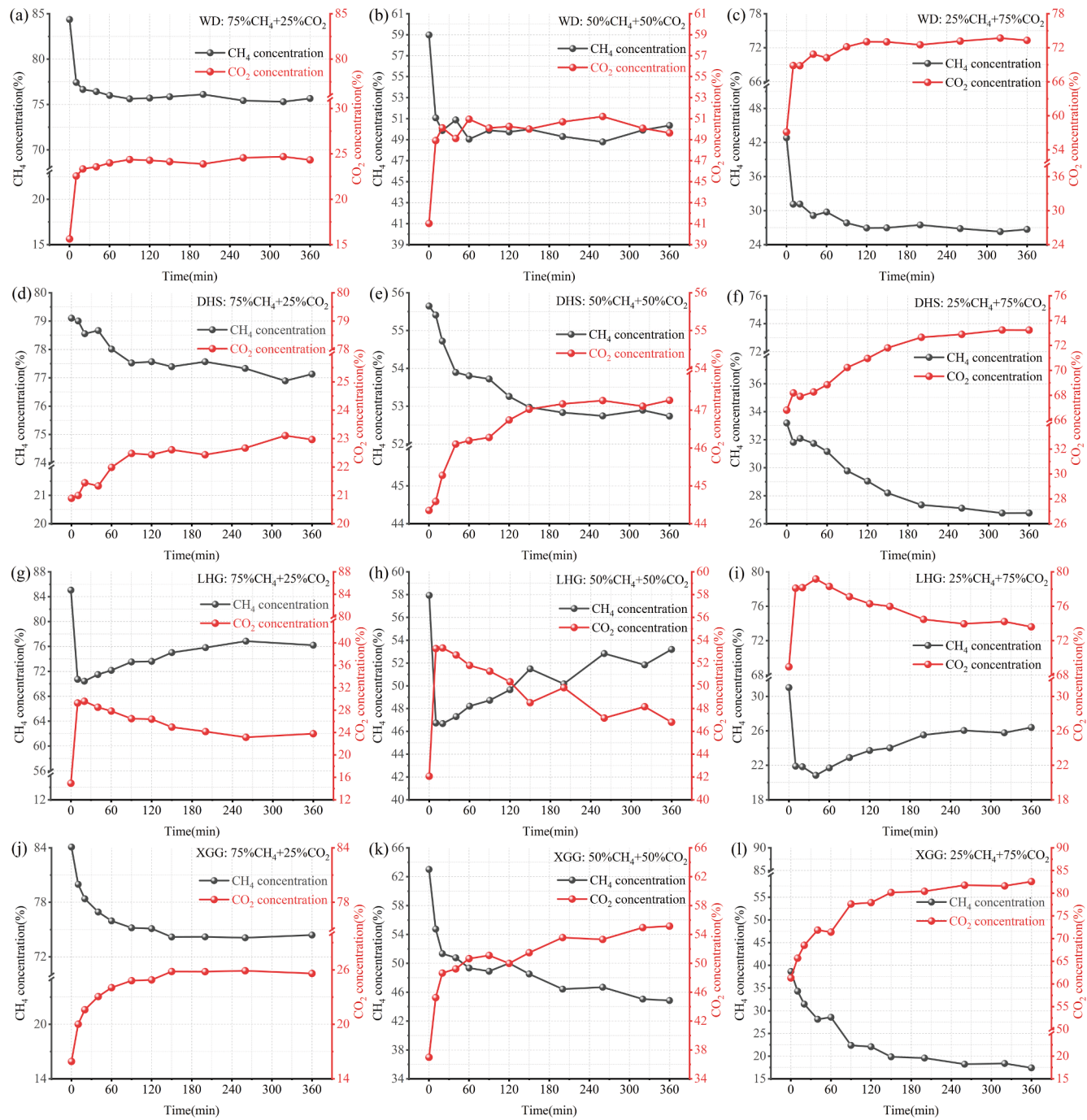


**Fig. 5.** Changes in composition over desorption time for different compositions ratios of CO<sub>2</sub>/CH<sub>4</sub>.

production mechanisms.

#### 4.1. Relationship between desorption volume and desorption strain

##### 4.1.1. Different samples with the same compositions ratios

Strain reflects the extent of deformation induced by adsorption/desorption in the coal matrix, thereby affecting the dynamic changes in permeability of coal reservoirs during ECBM processes [6,19]. The magnitude of desorption-induced contraction strain under constant temperature, pressure, and gas composition conditions is related to the deformability of the coal matrix [25,27]. Comparing the relationship between desorption volume and desorption strain for different samples under the same compositions ratios, it is observed that the DHS sample exhibits the highest strain under the same desorption volume, especially

under conditions of 100 % CH<sub>4</sub> and 25 % CO<sub>2</sub> + 75 % CH<sub>4</sub>, surpassing the other three samples (Fig. 6a, b). With the increase in CO<sub>2</sub> concentration, the pattern becomes more pronounced among different samples under the same desorption volume condition, with the overall deformability ranking as DHS > XGG > LHG > WD (Fig. 6).

The desorption strain of different samples exhibits a noticeable strain hysteresis effect as the desorption volume increases under different compositions ratios of CO<sub>2</sub>/CH<sub>4</sub>. Initially, desorption volume and desorption strain show a linear correlation. As the desorption volume gradually reaches equilibrium, the desorption volume stabilizes while the desorption strain continues to increase [28]. The strain hysteresis effect varies significantly among different samples, with LHG and DHS showing a more pronounced hysteresis, whereas WD and XGG samples exhibit a weaker hysteresis effect (Fig. 6).

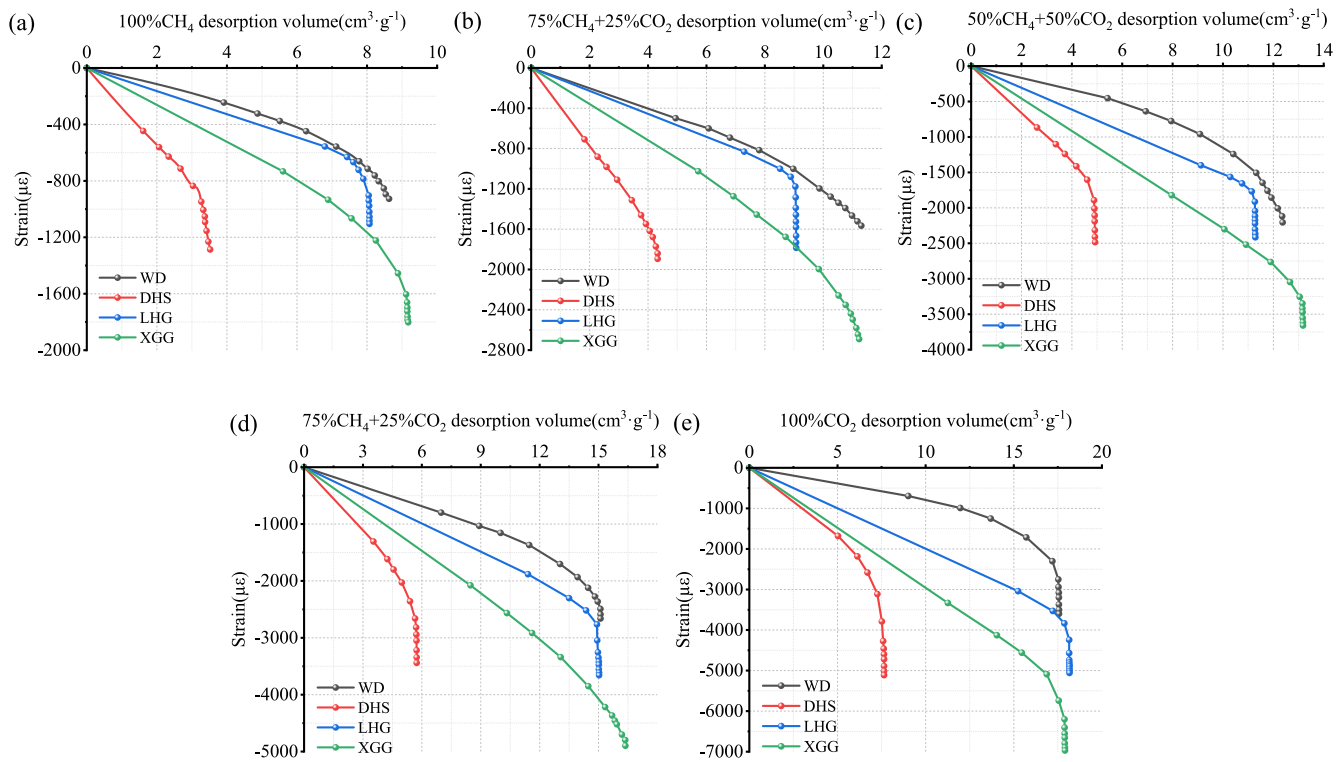


**Fig. 6.** Relationship between desorption volume and desorption strain with different samples.

#### 4.1.2. Different compositions ratios of $\text{CO}_2/\text{CH}_4$ for the same sample

With the increase in  $\text{CO}_2$  concentration, the desorption volume and desorption strain of different coal samples also increase (Fig. 7). Specifically, for WD and DHS samples, the variation in desorption strain

under the same desorption volume conditions is relatively small across different  $\text{CO}_2$  concentrations, which may be related to the weaker desorption-induced deformation ability of WD samples and the lower adsorption capacity of DHS samples (Fig. 7a, b). In contrast, for LHG and

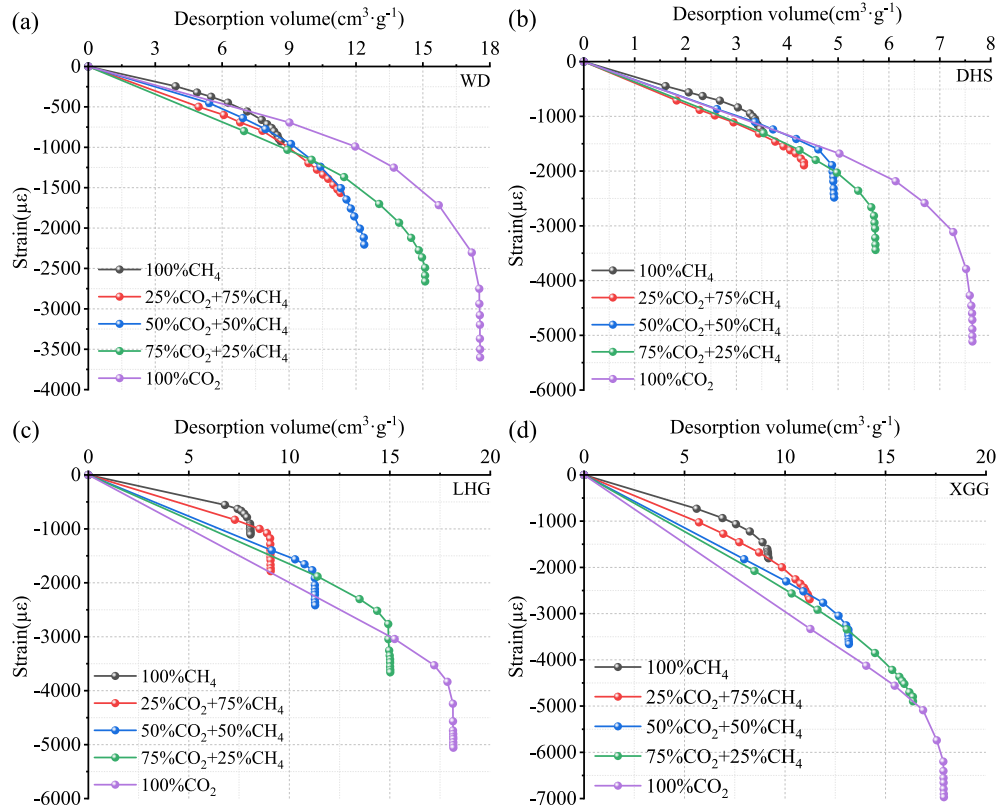


**Fig. 7.** Relationship between desorption volume and desorption strain under different compositions ratios of  $\text{CO}_2/\text{CH}_4$ .

XGG samples, the desorption strain increases with increasing CO<sub>2</sub> concentration under the same desorption volume, and this trend is more pronounced (Fig. 7c, d). This is associated with the tendency of CO<sub>2</sub> concentration to induce more significant matrix deformation during adsorption/desorption processes [29].

All samples exhibited more pronounced strain hysteresis effects and greater strain hysteresis amounts with increasing CO<sub>2</sub> concentration (Fig. 7). During the initial stage of desorption, as the desorption volume increases, the desorption strain also increases, and linearly correlated. However, in the later stage of desorption, the increase in desorption volume slows down, but the change in desorption strain remains significant, resulting in a pronounced strain hysteresis phenomenon. Different samples exhibit noticeable strain hysteresis effects under different compositions ratios of CO<sub>2</sub>/CH<sub>4</sub>.

#### 4.2. Characteristics of gas composition concentration changes during desorption process

Using the gas concentration at 0 min of desorption as the baseline, the characteristic changes in the concentration of different compositions ratios of CO<sub>2</sub>/CH<sub>4</sub> during the desorption process are calculated (Fig. 8). For the WD sample, there is a significant change in concentration during the initial stage of desorption (0–10 min). Under different compositions ratios of CO<sub>2</sub>/CH<sub>4</sub> (25 % CO<sub>2</sub> + 75 % CH<sub>4</sub>, 50 % CO<sub>2</sub> + 50 % CH<sub>4</sub>, 75 % CO<sub>2</sub> + 25 % CH<sub>4</sub>), the concentration changes are 6.94 %, 7.90 %, and 11.71 %, respectively. In the later stages of desorption, the changes in concentration are relatively small, with the changes at the end of desorption being 8.71 %, 8.62 %, and 16.15 % under the above conditions, respectively (Fig. 8a). During the desorption process, the concentration changes in DHS and XGG samples showed a steady increase over desorption time (Fig. 8b, d). The LHG sample exhibits different concentration change characteristics compared to the other three samples, with a large change in concentration during the initial stage of desorption, followed by a slow decrease (Fig. 8c). Overall, the changes in CH<sub>4</sub> and CO<sub>2</sub> concentrations during the desorption process of different

samples show a trend of rapid initial changes followed by slower changes (Fig. 8). This is determined by the effective diffusion rate during the desorption process [17,18].

There are differences in concentration changes among different samples. Under different compositions ratios of CO<sub>2</sub>/CH<sub>4</sub>, higher CO<sub>2</sub> concentrations result in larger changes in CH<sub>4</sub> and CO<sub>2</sub> concentrations during desorption. Moreover, the concentration change trends among the same samples under different compositions ratios of CO<sub>2</sub>/CH<sub>4</sub> are consistent (Fig. 8).

#### 4.3. Factors influencing the desorption rate

##### 4.3.1. Concentration characteristics

Desorption rate is a crucial parameter measuring the variation of desorption volume over time, indicating the volume of desorbed gas per unit time. To characterize the desorption rates of different coal samples under different compositions ratios of CO<sub>2</sub>/CH<sub>4</sub>, the Bangham model is utilized to fit their desorption processes [30]. Throughout the desorption processes, the desorption rates of different samples exhibit an exponential decrease trend, with overall desorption rates ranking as LHG > XGG > WD > DHS (Fig. 9).

The differences in desorption rates among different samples are significant, while within the same sample, different compositions ratios of CO<sub>2</sub>/CH<sub>4</sub> show that higher CO<sub>2</sub> concentrations correspond to higher desorption rates (Fig. 9). CO<sub>2</sub> molecules exhibit stronger adsorption compared to CH<sub>4</sub> molecules in competitive adsorption, making desorption more difficult. However, during CBM production, when reservoir pressure decreases, the adsorption equilibrium of multi-composition gases in the coal seam is disrupted. Different gas compositions compete to desorb from the pore-fracture surfaces and diffuse as free state. Compared to the diffusion process, the desorption time can be considered negligible [31]. Due to its linear molecular structure (O=C=O) and smaller kinetic diameter, CO<sub>2</sub> can enter smaller pores and fractures, resulting in a higher effective diffusion rate [32,33].

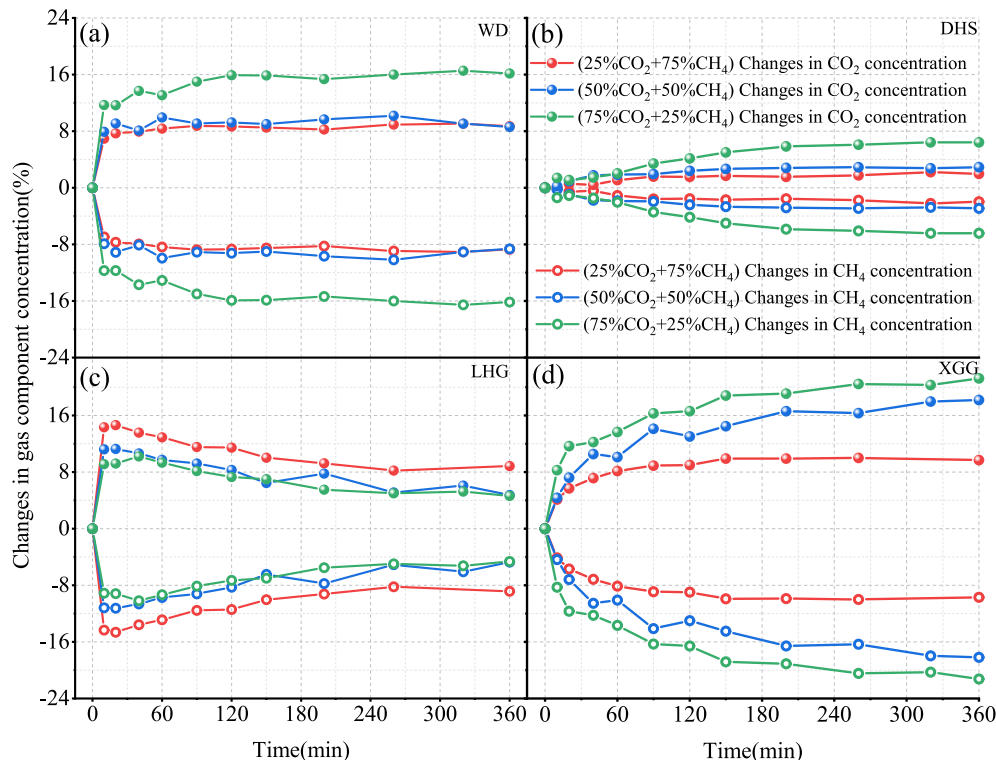


**Fig. 8.** The characteristic changes in CH<sub>4</sub> and CO<sub>2</sub> concentrations over desorption time.

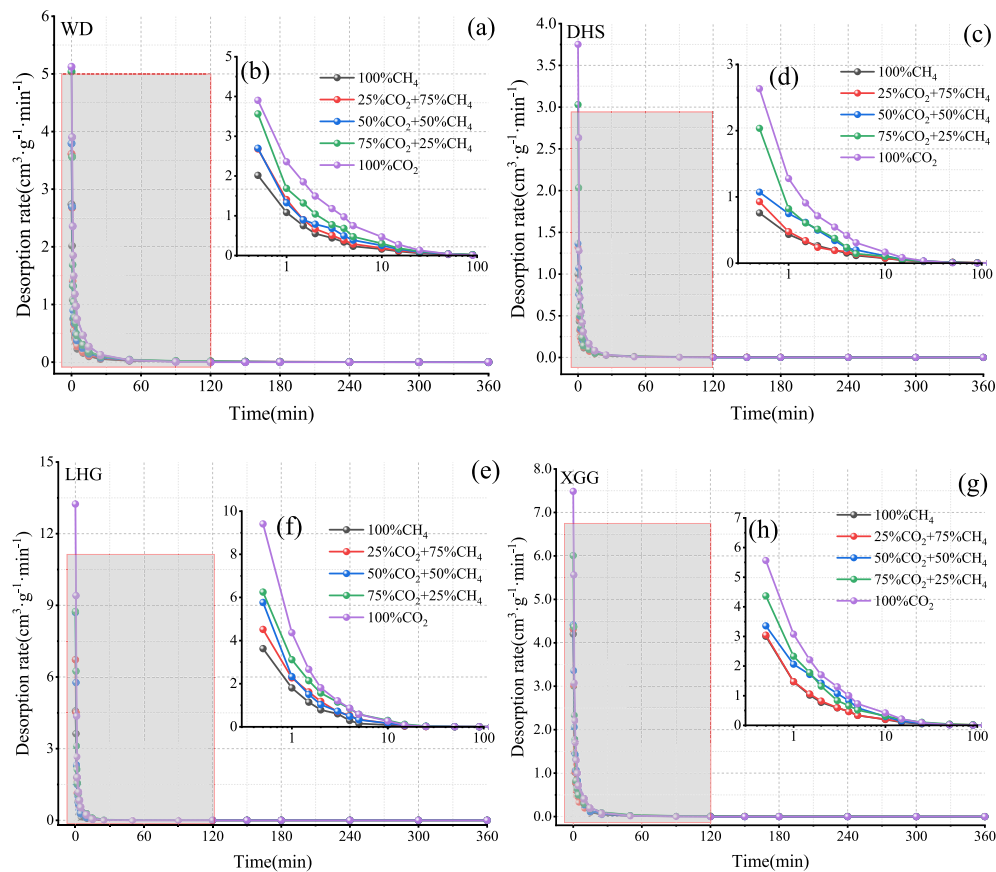


**Fig. 9.** Desorption rate curves under different compositions ratios of  $\text{CO}_2/\text{CH}_4$ .

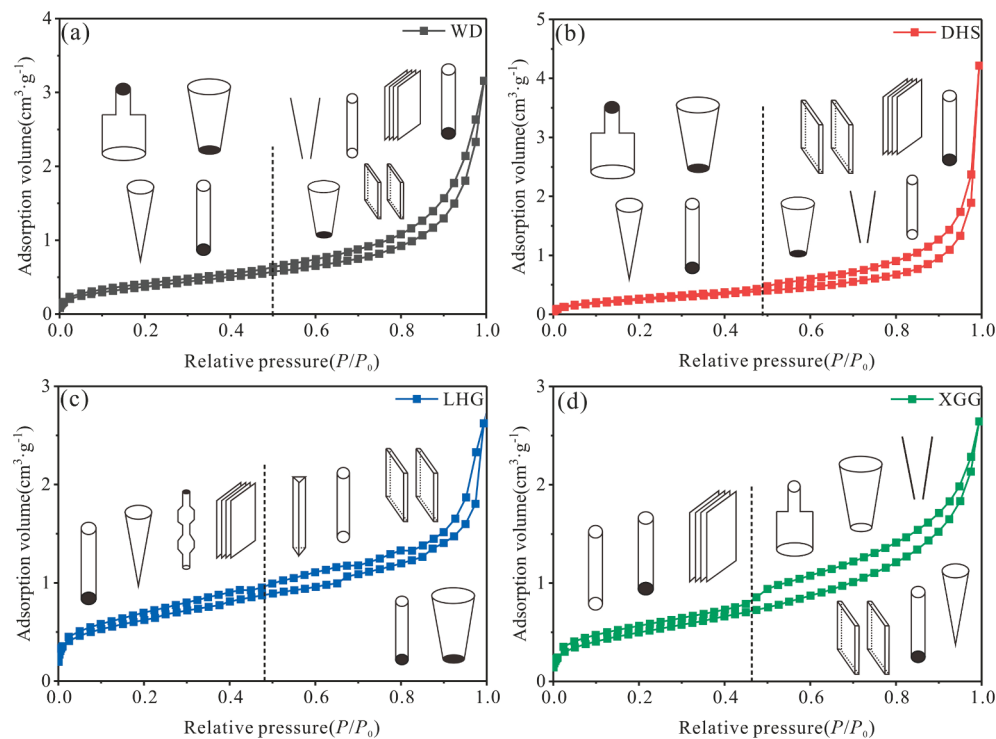


**Fig. 10.** Adsorption-desorption curves and pore structure characteristics of different coal samples.

#### 4.3.2. Pore structure

Under constant temperature and pressure conditions, pore structure characteristics (such as pore size and pore morphology) are crucial factors influencing gas diffusion [34]. To investigate the influence of pore size and morphology on gas diffusion during the production, low-temperature liquid nitrogen adsorption-desorption curve is utilized to analyze the pore morphology in different coal samples. The separation degree of adsorption-desorption curves can classify pore morphology into open pores, semi-closed pores, and closed pores. Further classification can be made based on the hysteresis loop morphology, distinguishing between cylindrical pores, parallel plate-like pores, and ink bottle-like pores [34,35].

The adsorption-desorption curves of different samples indicate that WD and DHS samples exhibit similar pore structure characteristics. In the low-pressure range ( $P/P_0 < 0.5$ ), the adsorption-desorption curves of WD and DHS samples approximately overlap, indicating that the predominant pore morphology is semi-closed pores. At high relative pressures ( $P/P_0 > 0.5$ ), hysteresis loops appear, suggesting that the pore structure consists mainly of conical pores and semi-closed pores, with a small amount of plate-like pores and cylindrical pores (Fig. 10a, b). For LHG and XGG samples, the adsorption-desorption curves are parallel but not fully coincident in the low-pressure range, indicating that composed of semi-open pores with one end closed and a small amount of cylindrical pores with both ends open (Fig. 10c, d). At high relative pressures, XGG sample exhibits more pronounced hysteresis loops compared to LHG sample, mainly due to the development of conical pores, parallel plate-like pores, and a small amount of ink bottle-like pores with both ends open. For semi-closed pores with poor opening degree, open pores are more conducive to diffusion behavior during CBM production [36]. XGG sample exhibits better opening degree compared to the other three samples, thus providing favorable diffusion pathways in terms of pore morphology.

The pore structure affects the difficulty level of diffusion, while pore size provides a more intuitive advantageous pathway for the migration of CBM [37,38]. The initial diffusion rate under different coal samples and different compositions ratios of  $\text{CO}_2/\text{CH}_4$  serve as the baseline to analyze the relationship between the initial diffusion rate and the total volume of mesopores and macropores. The results indicate that the larger the total volume of mesopores and macropores, the higher the diffusion rate of the corresponding samples (Fig. 11). The pore morphology of the XGG sample is more favorable for diffusion compared to other samples, while the LHG sample has the highest diffusion rate due to the significantly higher volume and proportion of mesopores and macropores, indicating that the pore volume of different pore sizes has a direct impact on diffusion.

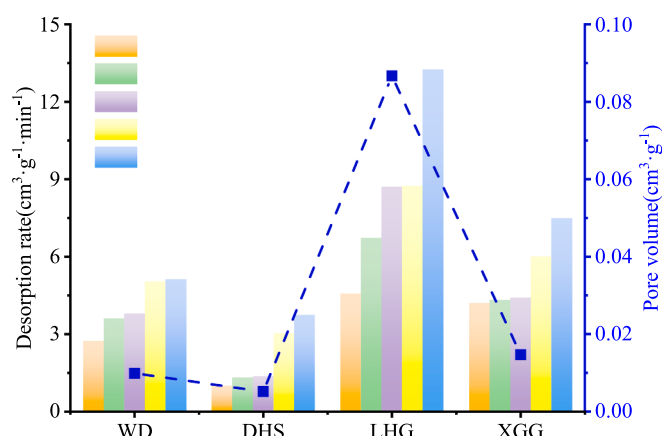


**Fig. 11.** The relationship between the initial diffusion rate and the pore volume of the seepage pore.

#### 4.4. $\text{CH}_4$ desorption characteristics at different compositions ratios

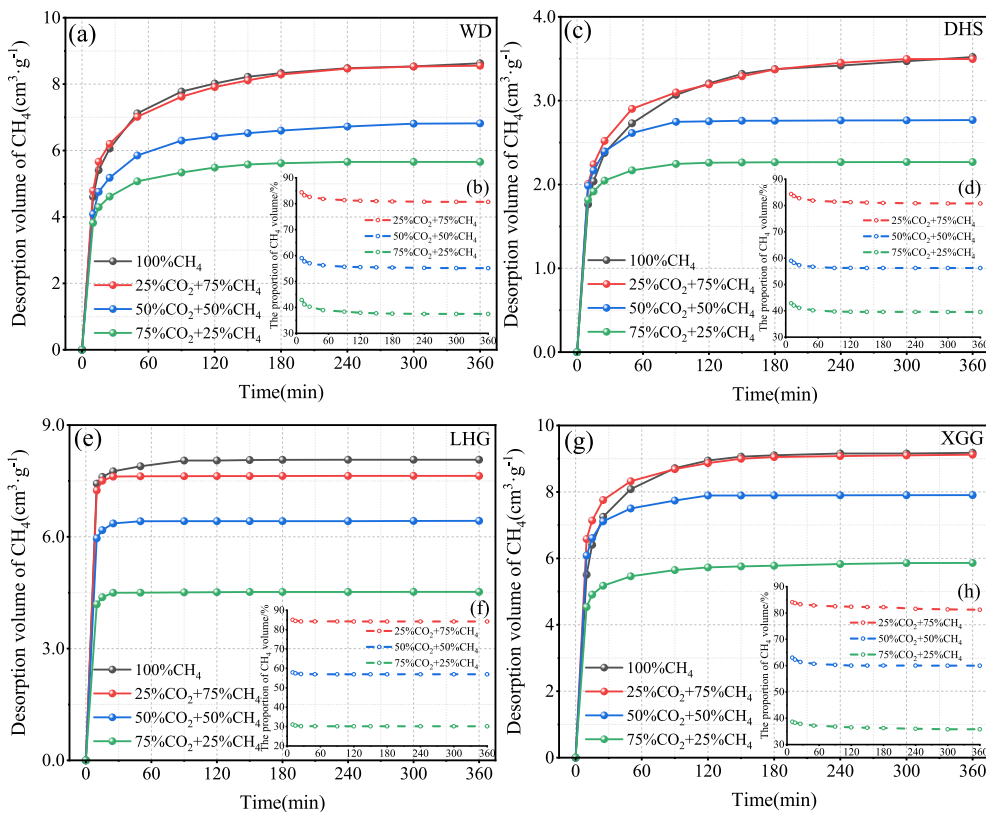
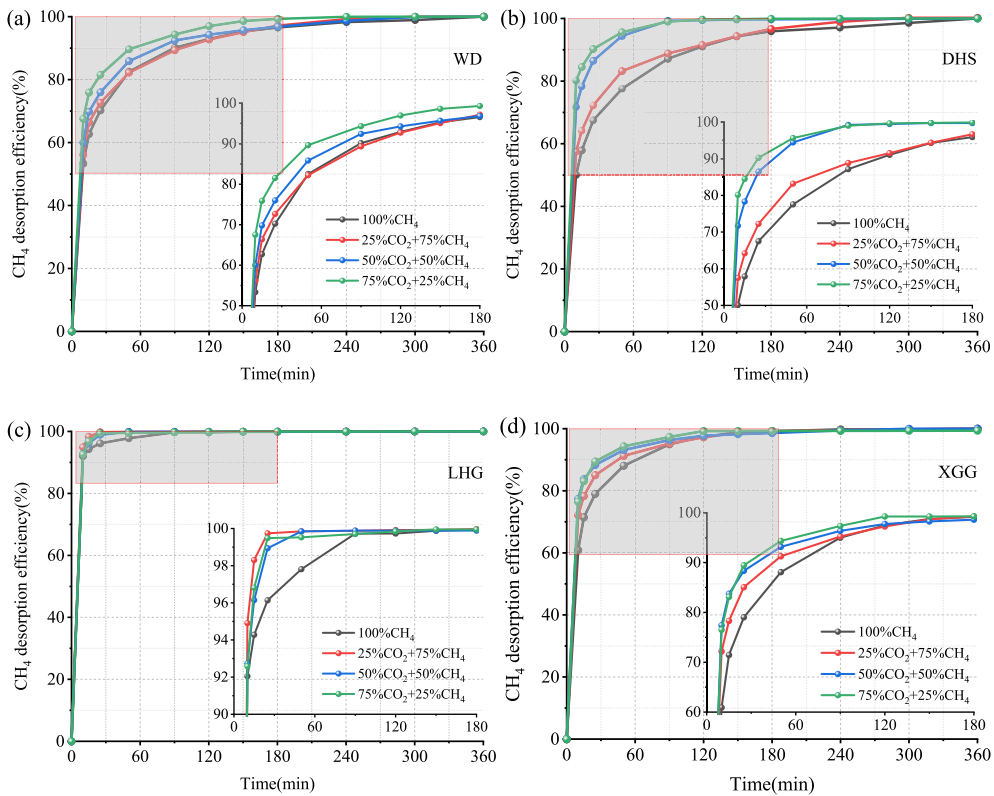
By calculating the  $\text{CH}_4$  desorption volume based on the concentration characteristics of different compositions ratios at various time intervals. It is observed that under different compositions ratios of  $\text{CO}_2/\text{CH}_4$ , the  $\text{CH}_4$  desorption curves are similar, showing a pattern of rapid desorption followed by slow desorption (Fig. 12). There are certain differences in  $\text{CH}_4$  desorption volumes among different samples under different compositions ratios. For instance, under different compositions ratios of  $\text{CO}_2/\text{CH}_4$  (100 %  $\text{CH}_4$ , 25 %  $\text{CO}_2 + 75\% \text{CH}_4$ , 50 %  $\text{CO}_2 + 50\% \text{CH}_4$ , 75 %  $\text{CO}_2 + 25\% \text{CH}_4$ ), the  $\text{CH}_4$  desorption volume for the WD sample is  $8.63 \text{ cm}^3 \cdot \text{g}^{-1}$ ,  $8.53 \text{ cm}^3 \cdot \text{g}^{-1}$ ,  $6.82 \text{ cm}^3 \cdot \text{g}^{-1}$ , and  $5.66 \text{ cm}^3 \cdot \text{g}^{-1}$ , respectively (Fig. 12a). The  $\text{CH}_4$  desorption volume under the 100 %  $\text{CH}_4$  and 25 %  $\text{CO}_2 + 75\% \text{CH}_4$  conditions are nearly identical, but significantly higher than the desorption volumes under the other two compositions ratios. This indicates that under low  $\text{CO}_2$  concentration conditions, the production of CBM wells is not significantly affected (Fig. 12a, c, e, g). Throughout the desorption process under different compositions ratios, the proportion of  $\text{CH}_4$  volume in the desorbed gas consistently remains higher than the initial ratio (Fig. 12b, d, f, h). In particular, under the 25 %  $\text{CO}_2 + 75\% \text{CH}_4$  condition, the proportion of  $\text{CH}_4$  volume in the desorbed gas remains consistently above 80 %, indicating that  $\text{CO}_2$  at different concentrations all has a promoting effect on  $\text{CH}_4$  production.

Based on the total  $\text{CH}_4$  desorption volume under different compositions ratios conditions, the efficiency of  $\text{CH}_4$  desorption at different time intervals is analyzed. Different  $\text{CO}_2$  concentration all promote the desorption of  $\text{CH}_4$  (Fig. 13).  $\text{CO}_2$  has different effects on the desorption efficiency of  $\text{CH}_4$  in different samples. WD and XGG samples both show a promoting effect on  $\text{CH}_4$  production under different compositions ratios, with higher  $\text{CO}_2$  concentrations leading to greater enhancement in  $\text{CH}_4$  production efficiency (Fig. 13a, d). Due to the absolute advantage of mesopores and macropores, the diffusion and migration pathways of  $\text{CH}_4$  are highly developed in the LHG sample. Therefore, the promoting effect of different  $\text{CO}_2$  concentrations on the production of  $\text{CH}_4$  is limited (Fig. 13c). The DHS sample has the smallest diffusion rate among different samples, resulting in a lower efficiency of  $\text{CH}_4$  production. However, under the displacement effect of high  $\text{CO}_2$  concentration, its production efficiency is significantly improved (Fig. 13b). Under different  $\text{CO}_2$  concentration conditions, there is a promoting effect on  $\text{CH}_4$  production efficiency, and the effect is more pronounced with higher  $\text{CO}_2$  concentrations. Among different samples,  $\text{CO}_2$  has a more significant promoting effect on samples where gas production is relatively difficult.

#### 4.5. Mechanism of $\text{CO}_2$ promoting $\text{CH}_4$ production

Previous studies on the adsorption behavior of different compositions gases under different reservoir conditions have confirmed that the adsorption affinity of different gas compositions in coal matrices is  $\text{CO}_2 > \text{CH}_4$  [3,9,39,40]. However, different gas compositions are not adsorbed independently in coal reservoirs. Instead, they exhibit competitive adsorption under different temperature and pressure conditions. The coal sample is under constant confining pressure during the desorption process. When the coal sample desorbs under atmospheric pressure conditions, the driving force for desorption is caused by the pressure drop. Specifically, during geological processes, as reservoir pressure decreases to atmospheric pressure, gases with relatively weak adsorption affinity, such as  $\text{CH}_4$ , preferentially desorb from the coal matrix surfaces and further diffuse into the coal fractures [34,41].

During the adsorption process of different compositions ratios of  $\text{CO}_2/\text{CH}_4$ , due to the significantly higher adsorption affinity of  $\text{CO}_2$  compared to  $\text{CH}_4$ , when reaching adsorption equilibrium, the  $\text{CO}_2$  in the adsorbed state is much higher than that of  $\text{CH}_4$ , while the  $\text{CH}_4$  in the free state dominates in the pore and fracture network (Fig. 14a). During desorption at atmospheric pressure, reservoir pressure drops to one

Fig. 12. CH<sub>4</sub> desorption volumes under different compositions ratios of CO<sub>2</sub>/CH<sub>4</sub>.Fig. 13. CH<sub>4</sub> production efficiency under different compositions ratios of CO<sub>2</sub>/CH<sub>4</sub>.

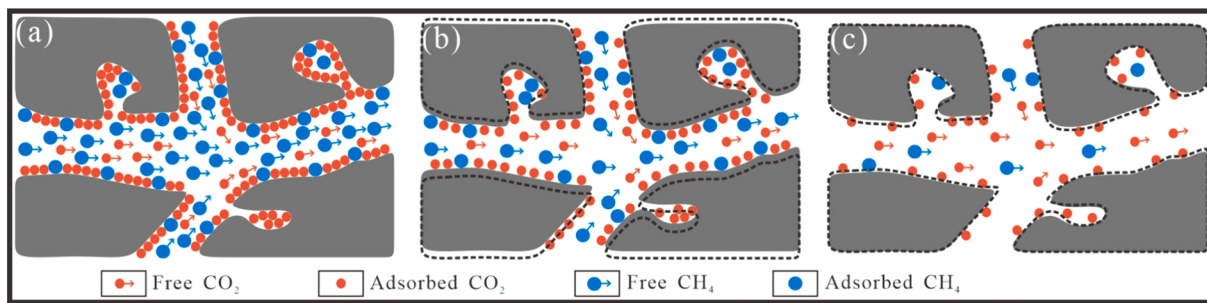


**Fig. 14.** Schematic diagram of phase changes during CO<sub>2</sub> and CH<sub>4</sub> co-desorption. (a) Adsorption (quasi) equilibrium stage; (b) main production stage of free gas (fracture pressure reduction stage); (c) desorption stage of adsorbed gas.

atmosphere in a very short time. Driven by pore pressure, a large amount of free gas is produced from fractures and large-pore pores, with the main composition being free-state CH<sub>4</sub> (Fig. 14b). As a large amount of free gas is produced, the effective stress increases sharply, compressing the pore-fracture system, which also leads to a rapid decrease in desorption strain in the early stages of desorption (Fig. 14b). After the free gas is produced and the reservoir pressure decreases, the adsorbed CH<sub>4</sub> and CO<sub>2</sub> begin to desorb, a process accompanied by matrix shrinkage effects [8,25] (Fig. 14c). Since the adsorption affinity of CO<sub>2</sub> is much higher than that of CH<sub>4</sub>, CH<sub>4</sub> desorbs earlier than CO<sub>2</sub> at the beginning of the desorption stage. As the volume of adsorbed CH<sub>4</sub> decreases, CO<sub>2</sub> begins to desorb, accompanied by a decrease in CH<sub>4</sub> concentration and an increase in CO<sub>2</sub> concentration.

## 5. Conclusion

Physical simulation experiments of desorption with different compositions ratios of CO<sub>2</sub>/CH<sub>4</sub> were conducted, and the desorption strain of coal samples and the dynamic changes in gas composition were monitored. The influencing mechanisms of dynamic changes in gas composition concentrations during desorption were analyzed.

- (1) For the same sample, during desorption of CO<sub>2</sub> and CH<sub>4</sub> at different compositions ratios, higher CO<sub>2</sub> concentrations resulted in greater desorption volumes and strains. Under the same desorption volume conditions, higher CO<sub>2</sub> concentrations led to greater desorption strains for different samples.
- (2) With increasing desorption time, the concentration of CH<sub>4</sub> gradually decreased while the concentration of CO<sub>2</sub> gradually increased, but CH<sub>4</sub> remains dominant in the desorption process. CO<sub>2</sub> promoted the production of CH<sub>4</sub>, and higher CO<sub>2</sub> concentrations resulted in higher CH<sub>4</sub> production efficiency.
- (3) The variation in concentration during desorption of different compositions ratios was influenced by the initial CO<sub>2</sub> concentration and pore structure. Higher CO<sub>2</sub> concentrations led to greater variations in concentration of different compositions during desorption. The desorption rate was influenced by the degree of pore openness and the volume of mesopores and macropores.

## CRediT authorship contribution statement

**Jielin Lu:** Writing – original draft, Methodology, Investigation, Formal analysis, Data curation, Conceptualization. **Xuehai Fu:** Writing – review & editing, Project administration, Methodology, Funding acquisition. **Junqiang Kang:** Supervision, Methodology. **Ming Cheng:** Supervision, Formal analysis. **Baoxin Zhang:** Supervision, Methodology. **Haifeng Ji:** Visualization, Data curation.

## Declaration of competing interest

The authors declare that they have no known competing financial interests or personal relationships that could have appeared to influence the work reported in this paper.

## Data availability

Data will be made available on request.

## Acknowledgements

This work was supported by the Major Science and Technology Projects in Xinjiang Uygur Autonomous Region (2022A03015-3, 2023A01004-3-2, 2023A01004-3-3), the National Natural Science Foundation of China (42372183, 42202198), the Natural Science Foundation of Jiangsu Province (BK20221149).

## References

- [1] Lan W, Wang H, Liu Q, et al. Investigation on the microwave heating technology for coalbed methane recovery. *Energy* 2021;237:121450.
- [2] Huang Q, Shen J, Zhang B, et al. Real-time monitoring of coalbed methane production network following liquid CO<sub>2</sub> injection in a low-efficiency well network: response to gas and water production characteristics. *Energy* 2023;285:129488.
- [3] Zhang L, Li J, Guo L, et al. Study on CO<sub>2</sub> Displacement Adsorption Behavior and Deformation Characteristics of Gas-Bearing Bituminous Coal. *J China Univ Min Technol* 2022;51(05):901–13.
- [4] Gentzis T. Subsurface sequestration of carbon dioxide—an overview from an Alberta (Canada) perspective. *Int J of Coal Geol* 2000;43(1–4):287–305.
- [5] Saghafi A, Faiz M, Roberts D. CO<sub>2</sub> storage and gas diffusivity properties of coals from Sydney Basin, Australia. *Int J of Coal Geol* 2007;70(1/3):240–54.
- [6] Sander R, Connell L, Pan Z, et al. Core flooding experiments of CO<sub>2</sub> enhanced coalbed methane recovery. *Int J Coal Geol* 2014;131:113–25.
- [7] Clarkson C, Bustin R. Binary gas adsorption/desorption isotherms: effect of moisture and coal composition upon carbon dioxide selectivity over methane. *Int J Coal Geol* 2000;42(4):241–71.
- [8] Majewska Z, Majewski S, Ziętek J. Swelling of coal induced by cyclic sorption/desorption of gas: experimental observations indicating changes in coal structure due to sorption of CO<sub>2</sub> and CH<sub>4</sub>. *Int J Coal Geol* 2010;83(4):475–83.
- [9] Sander R, Connell L, Camilleri M, et al. CH<sub>4</sub>, CO<sub>2</sub>, N<sub>2</sub> diffusion in Bowen Basin (Australia) coal: relationship between sorption kinetics of coal core and crushed coal particles. *J Nat Gas Sci Eng* 2020;81:103468.
- [10] Lama R, Saghafi A. Overview of gas outbursts and unusual emissions. In: The proceedings of coal 2002, 3rd Australian coal operators' conference, the Australasian institute of mining and metallurgy; 6–8 February 2002. p. 74–88.
- [11] Tang S, Tang D, Tao S, et al. CO<sub>2</sub>-enriched CBM accumulation mechanism for low-rank coal in the southern Junggar Basin. *China Int J of Coal Geol* 2022;253:103955.
- [12] Zhang B, Fu X, Wang Y, et al. Geochemical characteristics of gas/water in mixed genesis coalbed methane reservoirs and their application for gas production prediction. *J Clean Prod* 2023;418:138129.
- [13] Shi J, Durucan S, Fujioka M. A reservoir simulation study of CO<sub>2</sub> injection and N<sub>2</sub> flooding at the Ishikari coalfield CO<sub>2</sub> storage pilot project. *Japan Int J Greenh Gas Con* 2008;2(1):47–57.
- [14] Fujioka M, Yamaguchi S, Nakao M. CO<sub>2</sub>-ECBM field tests in the Ishikari Coal Basin of Japan. *Int J Coal Geol* 2010;82(3–4):287–98.
- [15] Cai Y, Shen J, Li C, et al. Principles and examples of CO<sub>2</sub>-ECBM site selection under the constraints of multiple geological attributes. *J China Coal Soc* 2020;45(12):4111–20.

- [16] Zhang Z, Liu G, Zhang X, et al. Adsorption-desorption experiment of CH<sub>4</sub>/CO<sub>2</sub> mixed gases with different concentrations. *J China Coal Soc* 2009;34(04):551–5.
- [17] Su X, Huang J, Wang Q, et al. Experimental study on CO<sub>2</sub>-enhanced coalbed methane production and its simultaneous sequestration. *Coal Geol Explor* 2023;51(01):176–84.
- [18] Moore T. Coalbed methane: a review. *Int J of Coal Geol* 2012;101:36–81.
- [19] Wang L, Wang Z, Li K, et al. Comparison of enhanced coalbed methane recovery by pure N<sub>2</sub> and CO<sub>2</sub> injection: experimental observations and numerical simulation. *J Nat Gas Sci Eng* 2015;23:363–72.
- [20] Pan J, Du X, Wang X, et al. Pore and permeability changes in coal reservoirs induced by true triaxial ScCO<sub>2</sub> fracturing based on low-field nuclear magnetic resonance. *Energy* 2024;286:129492.
- [21] Ross D, Bustin R. The importance of shale composition and pore structure upon gas storage potential of shale gas reservoirs. *Mar Petrol Geol* 2009;26(6):916–27.
- [22] Yang C, Zhang J, Wang X, et al. Nanoscale pore structure and fractal characteristics of a marine-continental transitional shale: a case study from the lower Permian Shanxi Shale in the southeastern Ordos Basin. *China Mar Petrol Geol* 2017;88:54–68.
- [23] Cui X, Bustin R, Dipple G. Selective transport of CO<sub>2</sub>, CH<sub>4</sub>, and N<sub>2</sub> in coals: insights from modeling of experimental gas adsorption data. *Fuel* 2004;83(3):293–303.
- [24] Zhang B, Fu X, Deng Z, et al. A comparative study on the deformation of unconfined coal during the processes of methane desorption with successively decreasing outlet pressure and with constant outlet pressure. *J Petrol Sci Eng* 2020;195:107531.
- [25] Wang Z, Fu X, Deng Z, et al. Investigation of adsorption-desorption, induced strains and permeability evolution during N<sub>2</sub>-ECBM recovery. *Nat Resour Res* 2021;1:1–18.
- [26] Pan J, He H, Li G, et al. Anisotropic strain of anthracite induced by different phase CO<sub>2</sub> injection and its effect on permeability. *Energy* 2023;284:128619.
- [27] Dai L, Pan Y, Xiao Y, et al. Parameter design method for distressing boreholes to mitigate roadway coal bursts: theory and verification. *Rock Mech Rock Eng* 2024.
- [28] Lv A, Aghighi M, Masoumi H, et al. On swelling stress-strain of coal and their interaction with external stress. *Fuel* 2022;311.
- [29] Wang Z, Fu X, Pan J. Effect of N<sub>2</sub>/CO<sub>2</sub> injection and alternate injection on volume swelling/ shrinkage strain of coal. *Energy* 2023.
- [30] Bangham D, Sever W. An experimental investigation of the dynamical equation of the process of gas-sorption. *Philos Mag* 1925;49(293):935–44.
- [31] Peter J, Beamish B, Marjorie V. Coalbed methane sorption related to coal composition. *Int J of Coal Geol* 1998;35(1–4):147–58.
- [32] Clarkson C, Bustin R. The effect of pore structure and gas pressure upon the transport properties of coal: a laboratory and modeling study. I. Isotherms and pore volume distributions. *Fuel* 1999;78(11):1333–44.
- [33] Zhang D, Cui Y, Li S, et al. Adsorption and diffusion behavior of methane and carbon dioxide in coals of different ranks. *J China Coal Soc* 2011;36(10):1693–8.
- [34] Cheng M, Fu X, Kang J, et al. Effect of water on methane diffusion in coal under temperature and pressure: a LF-NMR experimental study on successive depressurization desorption. *Fuel* 2022;324:124578.
- [35] Clarkson C, Solano N, Bustin R, et al. Pore structure characterization of North American shale gas reservoirs using USANS/SANS, gas adsorption, and mercury intrusion. *Fuel* 2013;103:606–16.
- [36] Zhang J, Wei C, Zhao C, et al. Effects of nano-pore and macromolecule structure of coal samples on energy parameters variation during methane adsorption under different temperature and pressure. *Fuel* 2021;289(1):119804.
- [37] Chalmers G, Bustin R, Power I. Characterization of gas shale pore systems by porosimetry, pycnometry, surface area, and field emission scanning electron microscopy/transmission electron microscopy image analyses: examples from the Barnett, Woodford, Haynesville, Marcellus, and Doig unitsCharacterization of Gas Shale Pore Systems. *AAPG Bull* 2012;96(6):1099–119.
- [38] Zhou S, Liu D, Cai Y, et al. Multi-scale fractal characterizations of lignite, subbituminous and high-volatile bituminous coals pores by mercury intrusion porosimetry. *J Nat Gas Sci Eng* 2017;44:338–50.
- [39] Faiz M, Saghafi A, Barclay S, et al. Evaluating geological sequestration of CO<sub>2</sub> in bituminous coals: the southern Sydney Basin, Australia as a natural analogue. *Int J Greenh Gas Con* 2007;1(2):223–35.
- [40] Jin H, Schimmelmann A, Mastalerz M, et al. Coalbed gas desorption in canisters: Consumption of trapped atmospheric oxygen and implications for measured gas quality. *Int J of Coal Geol* 2010;81(1):64–72.
- [41] Chen Y, Qin Y, Li Z, et al. Differences in desorption rate and composition of desorbed gases between undeformed and mylonitic coals in the Zhina Coalfield, Southwest China. *Fuel* 2019;239:905–16.